CRF neurons establish resilience via stress-history dependent BNST modulation

Authors:

Sherod E Haynes[1,2,3], Anthony Lacagnina[4*], Hyun Seo Seong[1*], Muhammad Afzal[5], Carole Morel[3], Aurelie Menigoz[1], Kanaka Rajan[5], Roger L Clem[4], Helen S Mayberg[5], Donald G. Rannie[1], Larry J. Young[1], Ming-Hu Han[3,4,6†]

Affiliations:

[1]Center for Translational Social Neuroscience, Yerkes National Primate Research Center, Department of Psychiatry and Behavioral Sciences, Emory University, Atlanta, GA 30322, USA

[2]Neuroscience Graduate Program, Emory University, Atlanta, GA 30322, USA

[3]Department of Pharmacological Sciences, Icahn School of Medicine at Mount Sinai, New York, NY 10029, USA

[4]Nash Family Department of Neuroscience and Friedman Brain Institute, Icahn School of Medicine at Mount Sinai, New York, NY, USA

[5]Nash Family Center for Advanced Circuit Therapeutics, Icahn School of Medicine at Mount Sinai, New York, NY, USA

[6]Department of Mental Health and Public Health, Faculty of Life and Health Sciences, Shenzhen Institute of Advanced Technology, Chinese Academy of Sciences, Shenzhen, Guangdong, China

*These authors contributed equally

[†]Corresponding electronic address: ming-hu.han@mssm.edu.

Abstract

Cumulative stress is a major risk factor for developing major depressive disorder (MDD), yet not everyone experiencing chronic stress develops MDD. In those who do not, it is unclear at what point, or by what mechanism, a trajectory of stable resiliency emerges. Utilizing a 10-day repeated social defeat stress model (RSDS) for MDD, we observed that a critical period between 7 and 10 daily defeats marks the phenotypical divergence of resilient from susceptible mice. In response to ongoing stress, corticotropin-releasing factor (CRF) neurons of the oval nucleus of the bed nucleus of the stria terminalis (BNSTov) display a sustained increased firing rate in resilient, but not susceptible mice. This neurophysiological adaptation was self-sustaining, but only after 7 critical stress exposures, indicating that the process of developing resilience is dependent on stress history. Our study reveals a novel process by which individuals might persist in the face of adversity by way of stress-provoked activation, not inhibition of a key CRF limbic region that establishes a pathway to resilience.

Major depressive disorder (MDD) is a crippling heterogeneous neuropsychiatric condition with high morbidity and lifetime prevalence, exacerbated by the ongoing global pandemic[1]. MDD is episodic in nature, with treatment success diminishing with each subsequent depressive episode[2]. Major life stressors are key risk factors for precipitating the onset of an episode[3,4]. While most people will report at least one major life stressor at some point in their lives, not everyone will go on to develop MDD. It is also known that depression can emerge after repeated significant stressor exposure, suggesting that cumulative exposure to stress is associated with increased depression risk in vulnerable individuals[5–8]. Cumulative stress causes numerous psychological insults that predispose neuropsychiatric conditions[5,9,10]. Many studies have explored the individual differences in stress susceptibility or resiliency, but the process critical to driving the divergence in phenotypes remain elusive. Recent studies suggest mechanisms involved in the emergence of depression may be distinct from those that maintain the depressive state[11,12]. With the odds of treatment failure increasing with subsequent depressive episodes,[2,13] and increased depression risk of cumulative stress, a potentially more effective strategy would be to target the mechanisms mediating resilience, enhancing the ability to cope with cumulative stress.

The ability to engage in social and hedonic-like behaviors in the face of psychosocial stress is an adaptive behavioral strategy, and failing to do so is associated with high morbidity[14–16]. Resiliency is defined as the "process of adapting well in the face of adversity… [to] threats, or significant sources of stress[15]." Resiliency is unlikely to emerge from the absence of a pathological stress response but instead is an active process involving a myriad of molecular, cellular and circuit-level changes in the brain. Repeated social defeat stress (RSDS) induces robust depression-like behavioral phenotypes in roughly 2/3 of mice[6,10]. The standard 10-day RSDS protocol has been employed widely to identify and study neurobiological features of susceptible and resilient subpopulations[6,7,17–23]. Studies on stress vulnerability often test

hypotheses after establishing vulnerable subgroups, making the processes that led to such phenotypic diversification unclear.

The Bed Nucleus of the Stria Terminalis (BNST) is an important node for integrating sensory cues, interoception, cognition, and motivational states to enact adaptive responses[24,25]. The BNST is well-positioned in the social salience network to integrate external cues with internal states to influence the outcome and context of social interactions[24–27]. The oval nucleus of the BNST (BNSTov) is a stress-sensitive subregion that is a key candidate region for encoding stress modulation of social behavior through its projections to areas such as the ventral tegmental area (VTA)[28–31] and dorsal raphe[32,33]. Corticotrophin-releasing factor (CRF) neurons of the BNSTov ($BNSTov^{CRF}$) are a significant output of this region and can influence affective states[34–37]. Since $BNSTov^{CRF}$ neurons are thought to promote arousal and adaptive responding according to stress-related changes in internal state[24,25,27,38–44], we hypothesized they might play a role in establishing resiliency to repeated social stress.

Using the 10-day RSDS paradigm, we used cell-type selective *ex vivo* electrophysiology, chemogenetics, optogenetics, and *in vivo* fiber photometry to interrogate the $BNSTov^{CRF}$ system to explore its role in the divergence of susceptible and resilient phenotypes. We observed that $BNSTov^{CRF}$ neurons encode repetitive social stress and undergo adaptation that coincides with the divergence of resilient and susceptible phenotypes. Unexpectedly, we observed that resiliency entails cumulative stress-history dependent neuroadaptive changes, whereas susceptibility emerges in the absence of similar adaptations. Activation of $BNSTov^{CRF}$ neurons using Designer-Receptors-Exclusively-Activated-by-Designer-Drugs (DREADDs) during social defeat led to a resilient phenotype while inhibition caused susceptibility. Finally, using RNAscope and optogenetics, we provide intriguing evidence for a potential role of *Crfr1* in $BNSTov^{CRF}$ neurons in mediating resilience.

53
54 **Results:**

55

56 **Susceptible vs. resilience phenotypes emerge between 7 and 10 daily episodes of social**
57 **defeat stress.**

58

59 RSDS produces divergent and enduring resilient/susceptible phenotypes following 10 episodes
60 of social defeat stress[6,21] has high ethological validity and enables the investigation of the
61 consequences of stress accumulation[5,7]. To examine the temporal divergences of resilient and
62 susceptible phenotypes in mice, a modified RSDS stress protocol was employed in which mice
63 were subjected to discrete numbers of social defeat episodes (SDEs) interspersed with social
64 interaction (SI), and sucrose preference (SP) tests administered after 1, 4, 7, and 10 SDEs (Fig.
65 1a-d). Social Interaction (SI) Ratio is a behavioral score of the SI test and measures the time
66 spent in the area proximal to the enclosure of a novel social target (social interaction zone). To
67 generate the SI ratio, interaction zone time is calculated both in the absence and presence of
68 the social target, such that SI ratio $\geqq 1$ is resilient and <1 is susceptible[21]. Surprisingly, we
69 found that the susceptible phenotype emerged between 7 and 10 SDEs, reflected by a robust
70 decrease in social interaction on day 10 compared to day 7 (Fig. 1e, Extended Data Fig 1a) (SI
71 ratio: 2.062 +/- 0.226 after 7 SDEs to 0.559 +/- 0.093, $p<0.0001$, n = 11 for susceptible and
72 1.967 +/- 0.188 (7 SDEs) to 1.554 +/- 0.163 (10 SDEs), p=0.2929, n=11 for resilient). There
73 were no significant differences in SI ratios after 7 SDEs between mice that went on to become
74 susceptible vs resilient after 10 SDEs (mean: 2.062 +/- 0.226 vs 1.967 +/- 0.188, two-tailed t-
75 test, p=0.7483, n= 11/group) (Extended Data Fig. 1b-c). To test whether this was a result of
76 repeated SI tests, in a separate experiment, we subjected independent groups of mice to either
77 1, 4, 7, or 10 SDEs, conducting the SI and SP tests only once, and observed a similar effect of
78 susceptible/resilient subgroups emerging after the seventh episode of social defeat (Extended

79 Data Fig. 2d-f). Resilient (10 SDEs) mice had an indistinguishable SI ratio from all mice after 7
80 SDEs, while susceptible (10 SDEs) mice had an SI ratio significantly lower than both groups
81 (Fig. 1f). In the SP test, resilient mice showed a similar preference for sucrose to all 7 SDE and
82 stress-naïve control mice. Susceptible mice, by contrast, exhibited a decreased SP relative to 7
83 SDE and resilient groups (Fig. 1g). Previous studies reported that RSDS produces susceptible
84 and resilient phenotypes after 10 SDEs in a bimodal distribution[21]. Here, we observed a
85 unimodal distribution of social interaction toward a novel conspecific in 7 SDE mice but a
86 bimodal distribution in 10 SDE mice, consistent with the emergence of distinct resilience and
87 susceptible phenotypes (Fig. 1h,i). The susceptible population of mice represents a statistically
88 distinct group compared to 7 SDE and 10 SDE resilient mice (Kolmogorov-Smirnov, $p<0.0001$;
89 Fig. 1j). The time spent interacting with a novel conspecific is significantly less in susceptible 10
90 SDE mice compared to the 7th SDE and 10th SDE resilient mice, which were indistinguishable
91 from each other (Fig.1k). The divergence into susceptible and resilient phenotypes was
92 dependent upon the number of SDEs, rather than the passage of time. Mice subjected to 7
93 consecutive days of social defeat stress displayed social approach behavior when tested on day
94 11 and day 30, yet when subjected to three additional defeat episodes, social avoidance
95 emerged (Extended Data Fig. 1g). Thus, it is the number of episodes (SDEs #8-10), not the
96 duration of time after the 7th SDE, that is responsible for the emergence of susceptible
97 phenotypes. To gain insight into potential neural mechanisms involved in the phenotypic
98 divergence, we used c-FOS immunohistochemistry as a proxy of neural activation in mice
99 subjected to 10 SDEs following a 30-minute social interaction with a non-aggressive novel
100 conspecific (Extended Data Fig. 2a). While several brain regions implicated in social behavior
101 and motivation were assessed, only the anterior dorsal BNST showed significant differences in
102 c-FOS immunoreactivity (c-FOS-ir) between the stress-naïve, susceptible, and resilient mice
103 (Extended Data Fig. 2b). Given its role in responding to chronic stress, valence, and

104 motivational processes, we more specifically examined the BNSTov[24]. While no difference in c-
105 FOS-ir was detected between stress-naïve and 7 SDE mice, there was a significant decrease in
106 c-FOS-ir in susceptible (10 SDEs) and a significant increase in resilient (10 SDEs) mice,
107 respectively (Extended Data Fig. 2c-e). Thus, the c-FOS-ir data suggests a neural divergence
108 in BNSTov in response to social threat that paralleled the divergence in SI defining resilient and
109 susceptible phenotypes.
110
111 **Divergence in BNSTov^{CRF} neuronal firing rates tracks the emergence of resilient and**
112 **susceptible phenotypes.**
113
114 CRF neurons of the BNST are a major output source of the oval BNST that are sensitive to
115 chronic stressors[27,45–47]. Thus, we hypothesized that chronic stress would alter BNSTov^{CRF}
116 neuronal activity coinciding with the divergence in resilient and susceptible behavioral
117 phenotypes. To test this hypothesis, *Crf*-ires-*Cre;*ai14 (tdTomato) mice[30,48–51] were subjected to
118 either 7 or 10 daily SDEs, and cell-attached *ex vivo* electrophysiological recordings were
119 conducted in the BNSTov (Fig. 2a,b). CRF$^+$, but not CRF$^-$, BNSTov neurons significantly
120 increased firing rate in 7 SDE mice compared to stress-naïve control mice. By contrast, CRF$^+$
121 firing in susceptible 10 SDE mice was indistinguishable from that of controls and was lower than
122 that of 7 SDE and resilient 10 SDE mice. CRF$^-$ neuron firing did not differ between groups (Fig.
123 2c,d). Moreover, there was a strong correlation between firing rate and social interaction ratio in
124 CRF$^+$ but not CRF$^-$ neurons in 10 SDE mice (CRF$^+$, R^2=0.5725, *p=0.0113; CRF- R^2=0.06096,
125 p=0.5219, Fig. 2e). CRF neurons display both burst and non-burst firing patterns[40,52,53] (Fig. 2f).
126 Burst firing patterns were prominent in resilient and 7 SDE mice, but few were seen in
127 susceptible and control mice (Fig. 2h). Additionally, percentage spikes within burst were higher
128 in 7 SDE and resilient compared to susceptible 10 SDE mice (***p=0.0004, one-way ANOVA,

129 Fig. 2i), but not susceptible or control mice. The number of spikes per burst and number of
130 bursts per cell was not significantly different amongst the groups (Fig. 2j,k). These data and
131 correlation analysis suggest the possibility that there is a causal link between the neuronal
132 activity of BNSTov^{CRF} neurons and the divergence of behavioral phenotypes.
133
134 **BNSTov^{CRF} neurons bidirectionally modulate the emergence of resiliency.**
135
136 To test the hypothesis that BNSTov^{CRF} neurons are regulating the maintained resiliency over the
137 last 3 episodes of RSDS, during which susceptible and resilient phenotypes emerge, we
138 injected *Crf*-ires-*Cre* mice with AAVs encoding Cre-dependent excitatory (DIO-hM3Dq),
139 inhibitory (DIO-hM4Di) DREADDs, or a control mCherry construct into the BNSTov and
140 administered CNO via drinking water[54–56] (Fig. 3a,b). We presaged that this experimental
141 design afforded the opportunity to modulate neurons over a longer time span than
142 intraperitoneal (IP) injections would allow with minimal invasiveness, particularly because it was
143 not clear over when neuroadaptation occurs within the 3-day window. mCherry control mice
144 exhibited both susceptible and resilient phenotypes (SI ratio <1.0 and ≧1.0, respectively) in
145 roughly the 60/40 ratio as expected[6,21] (Fig. 3c,f). Interestingly, mice injected with inhibitory DIO-
146 hM4Di displayed a robust susceptible phenotype, while DIO-hM3Dq mice displayed resilient
147 phenotypes following CNO drinking water administration (Fig. 3c). Moreover, none of the DIO-
148 hM4Di + CNO mice went on to develop resilience (0/10, SI >1.0) while 89% (8/9, SI ≧1.0) of
149 the DIO-hM3Dq were resilient (Fig 3c,f). Notably, the social defeat experience was not affected
150 by the DREADDs manipulations (Extended Data Fig. 3a, b). The SP test — a test of hedonic
151 behavior — revealed differences between mCherry susceptible (mCherry (S)) and resilient
152 (mCherry (R)) mice that were mirrored in DIO-hM4Di and hM3Dq mice, respectively. mCherry
153 (S) and hM4Di mice displayed a significant decrease in SP relative to mCherry (R) and hM3Dq-

154 injected mice (Fig. 3d). There were no significant differences in locomotion (Fig. 3e). The
155 chemogenetic manipulation also produced bidirectional effects on anxiety-like behavior in
156 elevated plus maze (EPM) and open-field tests (Extended Data Fig. 4). Surprisingly, mice
157 injected with hM3Dq-DREADDs went on to become resilient (Fig 3c) although activation of *Crf*
158 neurons of the BNST have previously been shown to produce depressive- and anxiogenic-like
159 responses[27,34,39,46,49,57]. Indeed in our hands, BNSTov^{CRF} activation produced social avoidance
160 in mice with low (0-1 social defeat) stress exposure replicating previous studies (Extended Data
161 Fig. 5). Interestingly, resilience only occurred as a result of BNSTov^{CRF} chemogenetic activation
162 between 7 and 10 episodes of social defeat; excitatory hM3Dq-DREADDs activation during
163 episodes 4-7 or 10-13 failed to display resiliency (Fig. 3g-i), suggesting stress history plays a
164 critical role in the behavioral outcomes of CRF modulation. Modulating *Crf* neurons with
165 inhibitory hM4Di- or excitatory hM3Dq- DREADDs between 8 and 10 SDEs led to enduring
166 susceptible or resilient phenotypes, respectively, up to 6 weeks after CNO manipulation
167 (Extended Data Fig. 6). These observations strongly support that the behavioral outcomes
168 induced by the activation of BNSTov^{CRF} neurons are stress-history dependent.
169

170 **Calcium dynamics underlying stress adaptation**

171 We combined fiber photometry with excitatory or inhibitory DREADDs to determine whether
172 SDE-induced neuroadaptation in BNSTov^{CRF} neurons, *in vivo*, reflects behavioral responses
173 consistent with resilient and susceptible phenotypes. Mice were co-injected with Cre-dependent
174 gCAMP7f and either DIO-hM4Di, -hM3Dq DREADDs or -mCherry viral vectors (Fig. 4a,b).
175 Clozapine-N-oxide (CNO) was administered via drinking water over the last 3 episodes of
176 RSDS, concomittant with the observed divergence of susceptible and resilient phenotypes.
177

178 In the control mice, we measured the calcium dynamics encoding social interaction with a novel
179 conspecific. In mice subjected to 7 SDEs, there was a decrease in neural activation upon
180 interaction in the mCherry (S/R) mice (Extended Data Fig. 7a). This pattern of activity occurred
181 in the presence and absence of a social target (no target/target trials) (Extended Data Fig. 7b).
182 Given that mice with shared stress-history of 7 SDEs appeared to have unimodal distribution on
183 a variety of measures, we hypothesized that calcium-encoded neural activity may diverge in
184 susceptible/resilient mice concomitant with the display of their respective behaviors on SI test.
185 Therefore, fiber photometric recordings were taken during SI Test 2 after mice after 10 SDEs.
186 Indeed, we observed mCherry (S) mice similarly had no change in the pattern of neural activity
187 between no target/ target trials, whereas mCherry (R) mice exhibited an increase in activity
188 upon social interaction (Extended Data Fig 7c). When comparing changes in calcium-encoded
189 neural dynamics between SI Test 1 and 2, mCherry (S) mice showed no difference, whereas
190 mCherry (R) mice developed an increase concomitant with the display of resilience (Fig. 4c-e).
191 These findings suggest that the persistence of neural activity across SDEs #8-10 is associated
192 with resiliency.
193
194 While we showed that we could bidirectionally drive the development of resilience/susceptibility,
195 this manipulation offers limited insight into the *in vivo* neural dynamics that reflect this
196 divergence point. To draw a link between neural changes and behavior *in vivo*, we multiplexed
197 chemogenetics and fiber photometry to bidirectionally drive the development of
198 resilient/susceptibility and mimic the neuroadaptive changes in BNSTov^{CRF} neurons that
199 produce behavioral divergence. During SI Test 1, similar to control mice, DREADDs injected
200 mice experienced a decreased in calcium-related neural activity upon initiating social interaction
201 with a novel conspecific (Extended Data Fig 7a), whose neural pattern was observed in both no
202 target and target trials (Extended Data Fig 7b). In hM4Di-injected mice, there were no
203 significant differences in neural activity during SI Test 1 and 2 trials, similar to control mCherry

204 (S) mice (Fig. 4f-h; Extended Data Fig. 7a-c). As was observed in the resilient (mCherry (R))
205 mice, the hM3Dq-injected group showed an increase in calcium-encoded neural activity (Fig 4f-
206 h). Mice injected with cre-dependent hM4Di showed a significant decrease in calcium-related
207 neural activity. In contrast, social interaction initiation led to increased activity in DIO-hM3Dq
208 injected mice (Fig. 4f-h). There were no significant differences in SI of mice subjected to 7
209 SDEs, yet differences emerge following 3 additional SDEs with a subset of mice becoming
210 susceptible and resilient (mCherry(R)/(S)) or activating/inhibiting DREADD promoting resiliency
211 and susceptibility in the direction predicted (Fig. 4i). We observed a strong correlation between
212 SI ratio and calcium activity only after 10 SDEs (Fig. 4j). There were no significant differences
213 observed in calcium-based neuronal activity upon social interaction with a novel conspecific in
214 mice subjected to 7 SDEs (Extended Data Fig. 7a,b), or in the absence of social interaction
215 (Extended Data Fig. 7d). In contrast, after 10 SDEs, mCherry (R) and DIO-hM3Dq injected
216 mice displayed significantly greater neuronal activation upon social contact relative to mCherry
217 (S) and DIO-hM4Di injected mice (Extended Data Fig. 7d). Despite the difference in time spent
218 interacting with a novel conspecific, the number of interaction zone entries were not significantly
219 different, nor differences in distance traveled (Fig. 4k, Extended Data Fig. 7e). These data
220 suggest that BNSTov^{CRF} neuronal dynamics are differentially altered by stress modulation in
221 accordance with phenotypical display resiliency/susceptibility.
222
223 ***Crfr1* expression in BNSTov^{CRF} neurons mirrors the behavioral emergence of resilience.**
224 We observed a stress-induced enhancement in firing rates of BNSTov^{CRF} neurons in resilient
225 mice. To explore the effect of this BNSTov^{CRF} stress modulation on CRF receptor transmission,
226 we used RNAScope *in situ* hybridization to quantify *Crfr1* and *Crfr2* in accordance with stress
227 history. Mice were subjected to either 7- or 10-daily episodes of social defeat, and the BNST
228 and *Crfr1* and *Crfr2* genes were assessed (Fig. 5a-c) due to their reported role in mediating
229 stress responses[30,58–60]. The percentage of CRFR1-expressing neurons among CRF-

230 expressing neurons was higher in mice subjected to 7 SDEs than in susceptible mice but not
231 significantly different than resilient mice (Fig. 5d). In contrast, there were no significant
232 differences in BNSTov neurons co-expressing *Crfr2 and Crf mRNA* across groups of mice (Fig.
233 5e). The overlap between *Crfr1* and *Crf* in the BNST was significantly greater in the oval
234 nucleus than in anterolateral, anteromedial, and ventral subregions of the anterior dorsal BNST
235 (Fig. 5c,f).
236
237 To explore the role of firing rate changes on gene expression and the development of resiliency,
238 we optogenetically stimulated BNSTov^{CRF} neurons using transgenic *Crf-Cre*::ai32 mice, which
239 express channelrhodopsin-2 (ChR2) in *Crf*-containing neurons [61] (Fig. 5g). For control
240 experiments, transgenic mice of a similar background were used, except instead of ai32, mice
241 expressed the tdTomato fluorophore in CRF neurons (*Crf-tdTomato*). 5 Hz stimulation
242 frequency was used in order to mirror the average firing rate observed in the spontaneous firing
243 rate of resilient mice (Fig. 2d). Mice received 15-minute 5 Hz photo-stimulation of BNSTov^{CRF}
244 neurons following physical stress on SDEs #8-10. Mice were placed in the adjacent
245 compartment separating the aggressor, preventing physical contact. The compartment divides
246 the aggressor cage in half by a clear plexiglass that allows for continuous sensory cues (Fig.
247 5h,i). Photo-stimulation of *Crf*::ChR2 mice led to a significantly higher SI ratio and greater
248 percentage resilient than *Crf::tdTomato* mice (89% vs. 33%) when stimulated during SDEs #8-
249 10 (Fig. 5j). Surprisingly, *Crf::ChR2* mice that received photo-stimulation but were not subjected
250 to SDEs #8-10 showed a significant decrease in SI ratio and 100% of the mice, becoming
251 susceptible (0/6, SI ≧ 1.0) (Fig. 5j). Photo-stimulation paired with SDEs #8-10 increased the
252 percentage of cells co-expressing *Crfr1* mRNA in CRF+ neurons relative to mice that
253 experienced photo-stimulation in the absence of additional stress (Fig. 5k, l). Additionally, we
254 obtained slice preparation from the optogenetically-induced resilient mice, and performed cell-

255 attached single unit recordings from BNSTov ChR2-expressing CRF neurons (Extended Data
256 Fig. 8a). Our recording data showed that optogenetic stimulation reliably induced 2.5 Hz, 5 Hz
257 and 10 Hz spike responses as expected (Extended Data Fig. 8b), and interestingly triggered
258 burst firing after the 5 Hz optical stimulation (Extended Data Fig. 8c,d). Importantly, Bath applied
259 CRFR1-selective antagonist NBI 27914 significantly decreased the firing rate of tested BNSTov
260 ChR2-expressing CRF neurons (Extended Data Fig. 8e,f). In summary, these data show that
261 maintenance of resiliency requires social defeat stress BNSTov^{CRF} activation and is correlated
262 with the upregulation of *Crfr1* expression in a stress-history dependent manner.
263
264 **Discussion**
265 The RSDS paradigm was modified to observe the effects of cumulative stress on neuroplasticity
266 in regions critical for mood regulation. Indeed, our work has uncovered a discrete window of
267 neuronal and behavioral plasticity between 7 and 10 SDEs during which susceptible and
268 resiliency phenotypes are established. Many of the studies investigating mechanisms of
269 susceptibility and resiliency have explored changes occurring after the 10 SDEs, when stable
270 susceptible/resilient phenotypes have already emerged. By capturing behavioral,
271 electrophysiological, and *in vivo* fiber photometric measures during the intra-social defeat stress
272 period, we uncover the mechanisms underlying the establishment of susceptible and resiliency
273 phenotypes, which may differ from those involved in its maintenance.
274
275 The BNST has been implicated in prosocial behaviors, and is a complex structure consisting of
276 16 different subnuclei serving separate functions[24,27,52,53]. While the oval nucleus has been
277 investigated in stress responses, we hypothesized that the region would be instrumental in
278 processing contexts associated with social stress. Indeed, we observed that individual
279 differences of stress effects on social behavior are encoded by BNSTov^{CRF} neurons. Prior

280 studies have implicated the overactivation of CRF neurons in the BNST as being pro-depressive
281 and anxiogenic[31,39,46,47,49], therefore, we were surprised to observe that BNSTov^{CRF} neurons
282 exhibited increased activity in resilient mice. Moreover, cell-type-specific activation of this CRF
283 neuronal population yielded resiliency in mice. Importantly, we were able to replicate the effects
284 of BNSTov^{CRF} activation, achieving a social avoidant response in line with previous studies, in
285 stress-naïve mice, suggesting that stress accumulation or stress history may play a critical role.
286 To our knowledge, this study is the first to target this neuronal population in a stress history-
287 dependent manner in the context of social behavior. While CRF or CRF neuronal involvement
288 in stress responding have been reported [20,62–64], it is unknown about the contribution of this
289 neuronal population to resilience establishment in the context of social behavior when stress is
290 increasingly accumulated. Indeed, we observed that the activating Cre-dependent hM3Dq
291 manipulation only produced resilient mice after a certain "dose" of daily stressors (7 SDEs),
292 suggesting that the BNSTov may be tightly modulated based on stress-history resulting in
293 adaptive responses in contexts where they may be most advantageous. Our findings support a
294 view that resilience is a stress history-dependent state, which does not exist prior to stress.
295 This is highly consistent with previous demonstrations that resilience is a status achieved by
296 active regulation of genes and ion channel functions in this group more than in susceptible
297 animals[21,65–67].
298
299 CRF neurons have been observed to influence the salience of stressful contexts according to
300 stress exposure[24,27,60,64,68]. One feasible mechanism by which this occurs is through CRF
301 receptor dynamics. We hypothesized that the development of resiliency or susceptibility occurs
302 via CRF-CRFR interactions in the BNST. We were surprised to observe *Crfr1* mRNA
303 expression in CRF neurons corresponded to the establishment of resilient/susceptible
304 phenotypes. CRFR1 has been found largely on non-CRF neurons in the BNST[68,69], but our

305 finding suggests that stress promotes *Crfr1* mRNA expression on CRF neurons themselves in a
306 stress-history-dependent manner. This is evidenced by there being a higher overlap of *Crfr1/Crf*
307 mRNA expression in mice subjected to 7 SDEs than in severely stressed mice that underwent
308 10 SDEs and became susceptible.
309
310 CRFR1 has been shown to be selectively activated in settings of stress following a chronic
311 stressor, serving as a signaler of ongoing stress[70]. Several studies using viral constructs to
312 overexpress CRF in the dorsolateral BNST led to a decrease in CRFR1, presumably as a
313 compensatory response, yet the behavioral consequences of this were not explored in the
314 context of susceptibility and resiliency to stress[34,35]. CRFR1 is a G_s-coupled receptor that leads
315 to strong depolarization promoting cell activation[36,46,70–72]. Therefore, these neurons establish
316 resiliency by way of prolonged activation of CRF neurons, in part, by the maintenance of
317 CRFR1 expression. This auto receptor-like ability has also been observed in terms of neuronal
318 activation. Chronic stress was shown to shift connectivity of local CRF^+ neurons from CRF^+-
319 CRF^- to a larger percentage of CRF^+-CRF^+ cells[73]. Studies using prolonged overactivation (over
320 weeks to months) of CRF activity have yielded antidepressant and anxiolytic results[29,34,35]. Here
321 we identify a more discrete timeline in the span of days to capture the transition of when
322 $BNSTov^{CRF}$ activation becomes pro-resilient. By optogenetically activating $BNSTov^{CRF}$ neurons,
323 we observed an increase in CRFR1 expression. Though correlative, this exquisite regulation of
324 CRFR1 according to stress-history and at times demonstrating an opposing effect on
325 depressive-like behavior, may underlie why clinical trials of CRFR1 antagonists for MDD have
326 been met with variable success[59,74–76]. Although beyond the scope of the current study, future
327 experiments using siRNA or CRISPR knockdown approaches should be performed to determine
328 whether upregulation of CRFR1 is a critical facet of neuroadaption leading to resiliency.
329

330 Stress-sensitive regions such as the BNST have been found to be of critical importance in
331 stress coping and reactivity[77–79]. Stress resilience has long been considered a response
332 separate from or in the absence of stimuli that gives rise to stress susceptibility, mediated by
333 parallel circuits or cell-types in a particular brain region[14,15,80]. Here, we observe that activity
334 dynamics of CRF neurons can shape and influence resiliency to stress, potentially through
335 (auto)regulation of *Crfr1* mRNA. Other substrates may be used to classify these neurons either
336 on the basis of dual-neuropeptide or circuit-specific identities and should be the object of future
337 exploration.
338
339 Previous work has shown that resiliency is influenced by dopaminergic VTA neurons in the
340 nucleus accumbens (NAc)[29], in part, through the actions of brain-derived-neurotrophic-factor
341 (BDNF)[21,81,82]. CRF peptide has been important for BDNF release in the NAc as a stress-
342 coincidence sensor[20], yet the sources of CRF important for altering stress effect on social and
343 hedonic behavior has not been extensively characterized. While long-range GABAergic BNST
344 neurons projecting to the VTA have been shown to influence reward and anxiety-like
345 behavior[48,83–86], it is unclear to what degree these cells comprise the oval nuclear BNST
346 population. The BNST also sends projections to the dorsal raphe, lateral and paraventricular
347 hypothalamus, and ventrolateral periaqueductal gray[27,31–33,42,77,87–89], among others, whose
348 modulation have been linked to stress on affect and social motivation. In this way, the BNST
349 acts as a node for integrating information regarding stress history and determining socio-
350 affective outcomes according, possibly due to CRFR1 receptor dynamics occurring on CRF
351 neurons of the oval nucleus, thereby shaping the long-lasting outcome of resiliency.
352
353 Our study highlights a previously unknown mechanism by which the BNST encodes cumulative
354 social stress and effectuates susceptible or resilient outcomes. Importantly, there are currently

355 no Food and Drug Administration-approved drugs aimed at preventing a depressive episode
356 from occurring. By targeting mechanisms involved in establishing resiliency, the possibility may
357 exist to therapeutically leverage windows of plasticity to effectuate resilience and evade the
358 development of MDD.
359

Methods

Mice

The study used wild-type, Crf-ires-Cre (Jackson labs: 011087), ai14 (Cre-responsive tdTomato reporter mouse; Jackson labs: 007915), ai32 (Cre-responsive channelrhodopsin-2/fused with eYFP; Jackson labs: 012569) mice on C57BL/6J background that were bred at Icahn School of Medicine at Mount Sinai and used were between 6-7 weeks at the start of experimental manipulations. Upon receipt from Jackson Laboratories, mice were acclimated to the housing facility for 1-2 weeks prior to the start of experiments. All mice were group-housed and maintained on a 12/12 light-dark cycle with ad libitum access to food and water. Following social defeat stress, mice were singly housed and maintained on a 12/12 light-dark cycle with ad libitum access to food and water. All experiments were approved by the Institutional Animal Care and Use Committee and comply with institutional guidelines for the Animal Care and Use Committee set forth by Icahn School of Medicine at Mount Sinai.

Repeated social defeat stress paradigm

The repeated social defeat stress paradigm was performed according to published protocols[6,21,23,82,90–92]. Briefly, CD1 aggressors were singly housed in cages (26.7 cm width x 48.3 cm depth x 15.2 cm height; Allentown Inc) at least 24 hours before the start of the experiment on one side with a clear perforated Plexiglas divider. Social stress consists of physical and sensory stress components. During the period which marks the physical stress, C57BL/6J mice are placed on the ipsilateral side of the cage as the CD1 aggressor for 10 minutes. Following this, the intruder mouse is placed in the contralateral side of the perforated Plexiglas divider for the remainder of the 24-hour period, marking the sensory-stress period. Every 24 hours, the intruder mouse is paired with a new aggressor for 10 episodes. Control mice were housed two mice per cage divided by a perforated Plexiglas divider and rotated and handled daily like the socially defeated mice.

388

389 **Social interaction test**

390 Social interaction testing was performed as described[6,20,21,65,66,81,82,93]. Briefly, a novel
391 conspecific of CD1 strain is placed in an interaction zone of a standard open-field arena, and
392 the time the intruder spends in the interaction zone is measured. The mice spend a total of 5
393 minutes in the open arena (2.5 min with and without the novel CD1). Ethovision (Noldus
394 Information Technology) video-tracking software is used to track interaction time. All social
395 interaction testing takes place 24 hours after the last defeat. Social interaction (SI) is measured
396 by time spent in the interaction zone during first (CD1 absent) over second (CD1 present) trials.
397 Mice are categorized according to SI ratios; an SI ratio ≧1 defines resilient, whereas an SI ratio
398 <1 is susceptible as described previously[5,17,19,21].

399

400 **Sucrose preference test**

401 For sucrose preference testing, a solution of 1% sucrose or diluent alone (drinking water) is filled
402 in 50 ml tubes with ball-pointed sipper nozzles (Ancare). Animals are acclimatized to two-bottle
403 choice conditions prior to testing. The bottles are weighed, and positions interchanged daily.
404 Sucrose preference is calculated as a percentage [100 x volume of sucrose consumed (in bottle
405 A)/total volume consumed (bottles A and B)] and averaged over 2 days of testing.

406

407 **Cell-attached electrophysiology**

408 Acute coronal brain slices of the BNSTov were prepared according to previously published
409 protocols[65,66,90,94]. All recordings were carried out blind to stress history, behavioral phenotype,
410 or drug treatment. Male 8-12 weeks old mice were perfused with cold artificial cerebrospinal
411 fluid (aCSF) containing (in mM): 128 NaCl, 3 KCl, 1.25 NaH_2PO_4, 10 D-glucose, 24 $NaHCO_3$, 2
412 $CaCl_2$, and 2 $MgCl_2$ (oxygenated with 95% O_2 and 5% CO_2, pH 7.35, 295-305 mOsm). Acute

413 brain slices containing BNSTov were cut using a microslicer (DTK-1000, Ted Bella) in sucrose-
414 ACSF, derived by replacing NaCl with 254 mM sucrose, and saturated by 95% O_2 and 5% CO_2
415 (2.5 ml/min) and 35ºC. Glass recording pipettes (2-4 MΩ) were filled with an internal solution
416 containing (mM): 115 potassium gluconate, 20 KCl, 1.5 $MgCl_2$, 10 phosphocreatine, 10 HEPES,
417 2 magnesium ATP and 0.5 GTP (pH 7.2, 285 mOSm). BNSTov CRF neurons were identified by
418 location, and infrared differential interference contrast microscopy and recordings were made
419 from CRF-positive neurons as indicated by the presence of tdTomato (in *Crf*::tdTomato mice) or
420 eYFP in the case of (*Crf*::ChR2) mice. Spontaneous firing rates were recorded in cell-attach
421 mode, and data acquisition and online analysis of firing rates were collected using a Digidata
422 1440 digitizer and pClamp 10.2 (Axon Instruments). The timing of recordings was made
423 consistent throughout treatment groups. A burst was defined as containing at least three
424 spikes, with interspike intervals <15 ms[95]. Neuronal firing rates were considered bursting or
425 non-bursting if they had undergone a statistically significant change with a $P<0.05$ on the rank-
426 sum test.
427
428
429 **Qualitative defeat assessment**
430 Social defeat encounters were recorded, and BORIS (Behavioral Observation Research
431 Interactive Software) was used to code behaviors. Five behaviors (cage exploration, aggressor
432 grooming, flight, motionless, rearing/defensive posturing) were scored per published reports on
433 typical social defeat behaviors[9,18,37,96]. The total time engaging in each behavior was tallied to a
434 blinded observer, and scores were aggregated.
435
436 **Viral constructs**
437 For DREADD experiments in CRF neuronal populations, CRF-ires-Cre animals were injected
438 with AAV5-hSyn-DIO-hM4D(Gi)-mCherry (Addgene: 44362-AAV5) (≥7x10^12), AAV5-hSyn-

439 DIO-hM3D(Gq)-mCherry (Addgene: 44361-AAV5) (≥7x10^12), and AAV5-hSyn-DIO-mCherry
440 (Addgene: 50459). For fiber photometric recordings, CRF-ires-Cre animals were injected with
441 AAV9-syn-FLEX-jGCaMP7f-WPRE (addgene: 104492-AAV9) (>1x10^12). All viruses were
442 purchased from Addgene.
443
444 **Stereotaxic virus and optic fiber implantation**
445 Under ketamine (80 mg/kg)/xylazine (10 mg/kg) anesthesia, mice were placed in a stereotaxic
446 frame (Kopf Instruments) and the BNSTov was targeted (coordinates: anterior/posterior +0.20,
447 media/lateral: +/- 2.15, dorsal/ventral, –4.0 mm; 15-degree angle). Hair was shaved around the
448 crown of the head, alcohol, and betadine were applied to the scalp. Ophthalmic ointment was
449 applied to the eyes to prevent dryness, a midline incision was made down the scalp, and a
450 craniotomy was made using a dental drill. A 10 ul Nanofil Hamilton syringe (WPI, Sarasota, Fl)
451 with a 34-gauge beveled metal needle was used to infuse 0.5 ul virus at a rate of 85 nl/minute.
452 Following infusion, the needle was kept at the injection site for 10 minutes and slowly
453 withdrawn. For the optogenetic experiments, chronically implantable optic fibers constructed
454 with 1.25 mm diameter, 200 um core, 0.39 numeral aperture (NA) were used (RWD). For the
455 fiber photometry experiments, chronically implantable optic fibers constructed with 1.25 mm
456 diameter, 400 um core 0.48 numerical aperture (NA) optic fiber and unilaterally implanted into
457 the BNSTov (coordinates: anterior/posterior +0.20, media/lateral: +/- 2.15, dorsal/ventral, –3.9
458 mm; 15º angle) (thor labs). Fiber optical ferrules were cemented to the skull using dental acrylic
459 (Parkell C&B Metabond). All optical stimulation and fiber photometric recording experiments
460 were conducted a minimum of 3-4 weeks post-implantation.
461
462 **CNO-drinking water construct**
463 Clozapine-N-Oxide (CNO) was obtained from (Hello Bio, catalog no HB6149). The dry chemical
464 was dissolved in drinking water obtained from the vivarium and diluted such that each mouse

465 received 5 mg/kg/day based on previous studies. CNO was made fresh each day for the three
466 days it was administered. CNO solutions were protected from light throughout the experimental
467 procedure. On average, mice consumed ~4-5 mL of water per day. Water bottles and mice
468 were weighed daily. CNO water bottles were exchanged for normal drinking water after the
469 social interaction test 1 and 8-12 hours before social defeat stress to ensure neuronal
470 modulation during stress exposure.
471
472 **Elevated plus-maze**
473 Mice began testing by being placed in the center of the maze (Model ENV-560A, Med
474 Associated, Fairfax, VT, USA), where movement was tracked using Ethovision behavioral
475 tracking software (Noldus). The test lasted 5 minutes.
476
477 **Open field test**
478 Mice were placed in an arena (42 cm (w) x 42 cm (d) x 42 cm (h); Nationwide Plastics, custom
479 order). Mice were tracked using behavioral tracking software (Ethovision, Noldus), and time
480 spent in the designated center and surround zone, as well as locomotor activity, were
481 measured.
482
483 **Optogenetic manipulation of BNSTov^{CRF} neurons**
484 Optical fibers were implanted on Ai32 (transgenic mouse line expressing light-gated cation
485 channel channelrhodopsin-2 (ChR2). Optical fiber Optogenetic stimulation was conducted via
486 the use of a diode-pumped solid-state (DPSS) 473-nm blue laser (Crystal Laser, BCL-473-050-
487 M), using a patch cord with an FC/PC adaptor (Doric Lenses, MFP_200/240/900-0.22_4m_FC-
488 MF2.5). A functional generator (Agilent Technologies; 33220A) was used to generate a 5 Hz
489 frequency, pulse width of 10 ms for 15 minutes[97,98], and power density between 7-9 mW mm$^{-2.}$
490 Experimenters were blinded to the stimulation group.

491 **Fiber photometry calcium imaging**

492 Optical recordings of GCaMP7f fluorescence were acquired using two LEDs at 490 and 405
493 (Thor Labs), reflected off dichroic mirrors (Semrock, FF495) and coupled into a 400 micro 0.48
494 NA optical fiber (Thorlabs BFH48-600) using a 40 x 0.48 NA microscope objective and fiber
495 launch with the pat chord linked to an implanted 400 um optical fiber with zirconia sheath.
496 Signals in both 470 and 405 nm channels are monitored throughout the recordings, whereas the
497 405 nm is used as an isosbestic control for ambient fluorescents and motion artifacts caused by
498 movement or torque about the fiber optic implant. Wavelengths were modulated at frequencies
499 of 210-220 and 330 Hz, respectively, with power output maintained at 20 mA and a DC offset of
500 3 mA for both light sources. All signalers were acquired at 1 kHz and lowpass filtered at 3 Hz.
501 Prior to social interaction testing, mice were handled for and connected via a patch cable and
502 placed in the home cage for 5-7 minutes for basal BNSTov recording and habituation prior to
503 the start of the no-target trial.

504

505 **Fiber photometry analysis**

506 A custom-written MATLAB code (modified from previously published work)[99] was used to
507 analyze the GCaMP7f signal. Firstly, the bulk fluorescent signal from both the 470 nm and 405
508 nm channels were normalized. A linear regression (slope of the 405 nm fitted against the 470
509 nm signal) was applied over the data to correct for bleaching of signal of the duration at each
510 recording. The Initial 3 seconds for the signals were discarded because of the
511 photoreceiver/LED rise time artifact. Detection of GCaMP7f signal is calculated as a change in
512 the 470 nm/fitted 405 nm signal over the fitted 405 signal ($\Delta F/F$). For the calculation of intensity
513 values around events of interest (PC2), a 6-second window was used. We used 3 seconds
514 before and after the PC2 event onset and computed z-scores for all such event windows.
515 These z-scored intensity values were then averaged within and between animals in particular
516 groups, and 95% confidence intervals for the averaged intensities were computed.

517

518 **RNAScope *in-situ* hybridization**

519 To prepare frozen sections, mice were placed in an air-tight chamber with 2.5 ml of isoflurane-
520 infused cotton balls. After 45-60 seconds (after respiratory depression and loss of
521 consciousness as evidenced by the negative tail and paw pinch), brains were acutely harvested
522 and placed in a -80°C storage chamber until RNAScope *in-situ* hybridization protocol
523 commenced. 16-µm coronal sections were collected on a cryostat (Leica Biosystems) at -20°C
524 and mounted directly onto ColorFrost Plus microscope slides (Fischer Scientific). Slides were
525 stored at -80°C until *in situ* hybridization (ISH) processing. ISH was performed using the
526 RNAscope multiplex fluorescent kit (Advanced Cell Diagnostics, ACD) according to the
527 manufacturer's instructions. The tissue was fixed in 4% paraformaldehyde (PFA) in PBS chilled
528 to 4°C for 15 minutes, washed twice briefly in 1x PBS, then dehydrated in 50% ethanol, 70%
529 ethanol, and twice in 100% ethanol for 5 minutes each at room temperature (RT). A
530 hydrophobic barrier was traced around sections of interest using an ImmEdge pen (Fischer
531 Scientific), and once the barrier dried, sections were incubated in Protease IV reagent for 30
532 minutes at RT, then rinsed twice in 1x PBS for 5 minutes. Probes for CRH and either CRHR1 or
533 CRHR2 (ACD) were warmed, mixed, and placed onto sections for hybridization at 40°C for 2
534 hours in a HybEZ II oven (ACD), which was used for all subsequent incubations. Sections were
535 washed twice in 1x wash buffer (ACD) for 2 minutes each, then incubated with a series of
536 amplification reagents at 40°C, Amp 1-FL for 30 minutes, Amp 2-FL for 15 minutes, Amp 3-FL
537 for 30 minutes, and Amp 4-FL Alt A or C for 15 minutes, washing twice in 1x wash buffer for 2
538 minutes each between steps. DAPI was applied to the sections for 30 s, then immediately
539 coverslipped with ProLong Gold mounting medium (Invitrogen).

540

541 Images were collected on a Zeiss LSM 780 confocal microscope at 20x, 40x, or 63x
542 magnification. mRNA puncta were quantified manually using FIJI 1.0 software (Image J), all
543 experimental conditions were blinded to the imager, and all cell analysis and quantification.
544
545 **Immunohistochemistry**
546 Mice were quickly anesthetized with urethane and perfused with cold 1x-PBS (OmniPure, Bio-
547 Rad) followed by cold 4% PFA (Fisher Hamilton Scientific). Brains were placed in PFA at 4ºC
548 for at least 24 hours, followed by being replaced with a 15% sucrose/PBS solution at 4ºC for 24
549 hours and brain sinking. The next day, brains were placed in a 30% sucrose/PBS solution at
550 4ºC for 24 hours. Once the brains sunk, it was washed in 1xPBS three times and mounted on a
551 freezing microtome for sectioning at 35 micrometers.
552
553 Sections were washed three times for 10 minutes in 1x PBS, then blocked in 5% bovine serum
554 albumin (Sigma-Aldrich) in 1x PBS with 0.3% Triton-X (Sigma-Aldrich) for 1 hour. Tissues were
555 incubated with primary antibodies for rabbit anti-mCherry ((1:1000), Invitrogen), rabbit anti-c-Fos
556 antibody (1:250, Milipore C-10, sc-271243) and goat anti-GFP (1:500, abcams) overnight at
557 4ºC. Sections were washed three times with 1xPBS and blocked with 0.3% Triton-X for one
558 hour. Tissue was blocked with secondary antibodies goat anti-rabbit/568 (1:1000, Abcams) and
559 donkey anti-goat Alexa-488 (1:500, Abcams) at room temperature for 1 hour. Sections were
560 washed three times with 1x PBS for 10 minutes and mounted on slides with ProLong Gold
561 antifade reagent with DAPI (invitrogen, P36931). Z-stacked images were acquired with a Zeiss
562 LSM780 multi photon confocal system and z-stacks were collated using ImageJ (Fiji). Cell
563 counters were obtained using the Cell Counter feature on ImageJ.
564
565

566 **Statistical analysis**

567 Animals were randomly assigned to control and experimental groups and all experimenters
568 were blinded. Mice were excluded if viral infection was off-target. No data was excluded for
569 other reasons. Student's two-tailed t-tests were used for comparisons of two experimental
570 groups. For parametric data sets, comparisons among three or more groups were performed
571 using one or two-way ANOVA tests followed by Tukey's or Bonferroni posthoc tests. For all
572 tests, $p<0.05$ was determined to be significant. Statistical analyses were performed using
573 Graph Pad Prism 9 .3.1 software (La Jolla, CA, USA). For data not normally distributed, non-
574 parametric analyses were performed.

575

576 **Data & Code availability**

577 All source data for this manuscript and MATLAB code used to analyze photometry data is
578 available upon request.

579
580 **Acknowledgements**
581
582 We would like to thank S.M. for generous sharing for input on the manuscript. We would like to
583 thank S.R. and L.L. for lending viral constructs for behavioral validation. We would like to thank
584 the animal care staff at ISMMS for the animal care staff and technical support. This research
585 was funded by the National Institutes of Health grants R01MH072908 to DGR and LJY,
586 R01MH1206387 to MHH and SJR, R21MH112081 to MHH and SJR, F31MH114624 to SEH,
587 and P51 OD011132 to YNPRC, by the National Key R&D Program of 1034 China No.
588 2021ZD0202900 to MHH.

589 **References**

590 1. Veer, I. M. *et al.* Psycho-social factors associated with mental resilience in the Corona
591 lockdown. *Transl. Psychiatry* **11**, 67 (2021).

592 2. Post, R. M. Transduction of psychosocial stress into the neurobiology of recurrent
593 affective disorder. *Am. J. Psychiatry* **149**, 999–1010 (1992).

594 3. Gold, P. W. Evidence that stress per se has a role in the precipitation and natural history
595 of depressive illness. *Mol. Psychiatry* **18**, 954–956 (2013).

596 4. Kendler, K. S., Karkowski, L. M. & Prescott, C. A. Causal relationship between stressful life
597 events and the onset of major depression. *Am. J. Psychiatry* **156**, 837–841 (1999).

598 5. Barthas, F. *et al.* Cumulative Effects of Social Stress on Reward-Guided Actions and
599 Prefrontal Cortical Activity. *Biol. Psychiatry* **88**, 541–553 (2020).

600 6. Golden, S. A., Covington, H. E., Berton, O. & Russo, S. J. A standardized protocol for
601 repeated social defeat stress in mice. *Nat. Protoc.* **6**, 1183–1191 (2011).

602 7. Martinez, M., Phillips, P. J. & Herbert, J. Adaptation in patterns of*c-fos* expression in the
603 brain associated with exposure to either single or repeated social stress in male rats.
604 *European Journal of Neuroscience* **10**, 20–33 (1998).

605 8. Zheng, Z. *et al.* Hypothalamus-habenula potentiation encodes chronic stress experience
606 and drives depression onset. *Neuron* (2022) doi:10.1016/j.neuron.2022.01.011.

607 9. Kudryavtseva, N. N., Bakshtanovskaya, I. V. & Koryakina, L. A. Social model of depression
608 in mice of C57BL/6J strain. *Pharmacol. Biochem. Behav.* **38**, 315–320 (1991).

609 10. Laine, M. A. *et al.* Brain activation induced by chronic psychosocial stress in mice. *Sci.*
610 *Rep.* **7**, 15061 (2017).

611 11. Hultman, R. *et al.* Brain-wide Electrical Spatiotemporal Dynamics Encode Depression
612 Vulnerability. *Cell* **173**, 166-180.e14 (2018).

613 12. Drysdale, A. T. *et al.* Resting-state connectivity biomarkers define neurophysiological
614 subtypes of depression. *Nat. Med.* **23**, 28–38 (2017).

615 13. Samuels, B. A. *et al.* Modeling treatment-resistant depression. *Neuropharmacology* **61**,
616 408–413 (2011).

617 14. Franklin, T. B., Saab, B. J. & Mansuy, I. M. Neural mechanisms of stress resilience and
618 vulnerability. *Neuron* **75**, 747–761 (2012).

619 15. Russo, S. J., Murrough, J. W., Han, M.-H., Charney, D. S. & Nestler, E. J. Neurobiology of
620 resilience. *Nat. Neurosci.* **15**, 1475–1484 (2012).

621 16. Karatsoreos, I. N. & McEwen, B. S. Psychobiological allostasis: resistance, resilience and
622 vulnerability. *Trends Cogn Sci (Regul Ed)* **15**, 576–584 (2011).

623 17. Laine, M. A. *et al.* Genetic Control of Myelin Plasticity after Chronic Psychosocial Stress.
624 *eNeuro* **5**, (2018).

625 18. Markham, C. M., Norvelle, A. & Huhman, K. L. Role of the bed nucleus of the stria
626 terminalis in the acquisition and expression of conditioned defeat in Syrian hamsters.
627 *Behav. Brain Res.* **198**, 69–73 (2009).

628 19. Gururajan, A., Bastiaanssen, T. F. S., Ventura Silva, A. P., Moloney, G. M. & Cryan, J. F.
629 The impact of psychosocial defeat stress on the BNST transcriptome in adult male mice.
630 *Eur. J. Neurosci.* (2021) doi:10.1111/ejn.15567.

631 20. Walsh, J. J. *et al.* Stress and CRF gate neural activation of BDNF in the mesolimbic reward
632 pathway. *Nat. Neurosci.* **17**, 27–29 (2014).

633 21. Krishnan, V. *et al.* Molecular adaptations underlying susceptibility and resistance to
634 social defeat in brain reward regions. *Cell* **131**, 391–404 (2007).

635 22. Matsuda, S. *et al.* Persistent c-fos expression in the brains of mice with chronic social
636 stress. *Neurosci. Res.* **26**, 157–170 (1996).

637 23. Berton, O. *et al.* Essential role of BDNF in the mesolimbic dopamine pathway in social
638 defeat stress. *Science* **311**, 864–868 (2006).

639 24. Waraczynski, M. Toward a systems-oriented approach to the role of the extended
640 amygdala in adaptive responding. *Neurosci. Biobehav. Rev.* **68**, 177–194 (2016).

641 25. Flanigan, M. E. & Kash, T. L. Coordination of social behaviors by the bed nucleus of the
642 stria terminalis. *Eur. J. Neurosci.* (2020) doi:10.1111/ejn.14991.

643 26. Lebow, M. A. & Chen, A. Overshadowed by the amygdala: the bed nucleus of the stria
644 terminalis emerges as key to psychiatric disorders. *Mol. Psychiatry* **21**, 450–463 (2016).

645 27. Daniel, S. E. & Rainnie, D. G. Stress modulation of opposing circuits in the bed nucleus of
646 the stria terminalis. *Neuropsychopharmacology* **41**, 103–125 (2016).

647 28. Jennings, J. H. *et al.* Distinct extended amygdala circuits for divergent motivational
648 states. *Nature* **496**, 224–228 (2013).

649 29. Dedic, N. *et al.* Chronic CRH depletion from GABAergic, long-range projection neurons in
650 the extended amygdala reduces dopamine release and increases anxiety. *Nat. Neurosci.*
651 **21**, 803–807 (2018).

652 30. Chen, Y., Molet, J., Gunn, B. G., Ressler, K. & Baram, T. Z. Diversity of Reporter
653 Expression Patterns in Transgenic Mouse Lines Targeting Corticotropin-Releasing
654 Hormone-Expressing Neurons. *Endocrinology* **156**, 4769–4780 (2015).

655 31. Dabrowska, J., Martinon, D., Moaddab, M. & Rainnie, D. G. Targeting Corticotropin-
656 Releasing Factor Projections from the Oval Nucleus of the Bed Nucleus of the Stria
657 Terminalis Using Cell-Type Specific Neuronal Tracing Studies in Mouse and Rat Brain. *J.*
658 *Neuroendocrinol.* **28**, (2016).

659 32. Matthews, G. A. *et al.* Dorsal raphe dopamine neurons represent the experience of
660 social isolation. *Cell* **164**, 617–631 (2016).

661 33. Marcinkiewcz, C. A. *et al.* Serotonin engages an anxiety and fear-promoting circuit in the
662 extended amygdala. *Nature* **537**, 97–101 (2016).

663 34. Regev, L. *et al.* Prolonged and site-specific over-expression of corticotropin-releasing
664 factor reveals differential roles for extended amygdala nuclei in emotional regulation.
665 *Mol. Psychiatry* **16**, 714–728 (2011).

666 35. Sink, K. S. *et al.* Effects of continuously enhanced corticotropin releasing factor
667 expression within the bed nucleus of the stria terminalis on conditioned and
668 unconditioned anxiety. *Mol. Psychiatry* **18**, 308–319 (2013).

669 36. Konishi, S., Kasagi, Y., Katsumata, H., Minami, S. & Imaki, T. Regulation of corticotropin-
670 releasing factor (CRF) type-1 receptor gene expression by CRF in the hypothalamus.
671 *Endocr. J.* **50**, 21–36 (2003).

672 37. Jasnow, A. M., Banks, M. C., Owens, E. C. & Huhman, K. L. Differential effects of two
673 corticotropin-releasing factor antagonists on conditioned defeat in male Syrian hamsters
674 (Mesocricetus auratus). *Brain Res.* **846**, 122–128 (1999).

675 38. Avery, S. N., Clauss, J. A. & Blackford, J. U. The human BNST: functional role in anxiety
676 and addiction. *Neuropsychopharmacology* **41**, 126–141 (2016).

677 39. Kim, S.-Y. *et al.* Diverging neural pathways assemble a behavioural state from separable
678 features in anxiety. *Nature* **496**, 219–223 (2013).

679 40. Rodríguez-Sierra, O. E., Goswami, S., Turesson, H. K. & Pare, D. Altered responsiveness of
680 BNST and amygdala neurons in trauma-induced anxiety. *Transl. Psychiatry* **6**, e857
681 (2016).

682 41. Ventura-Silva, A. P. *et al.* Stress shifts the response of the bed nucleus of the stria
683 terminalis to an anxiogenic mode. *Eur. J. Neurosci.* **36**, 3396–3406 (2012).

684 42. Giardino, W. J. *et al.* Parallel circuits from the bed nuclei of stria terminalis to the lateral
685 hypothalamus drive opposing emotional states. *Nat. Neurosci.* **21**, 1084–1095 (2018).

686 43. Duvarci, S., Bauer, E. P. & Paré, D. The bed nucleus of the stria terminalis mediates inter-
687 individual variations in anxiety and fear. *J. Neurosci.* **29**, 10357–10361 (2009).

688 44. Duque-Wilckens, N. *et al.* Extrahypothalamic oxytocin neurons drive stress-induced
689 social vigilance and avoidance. *Proc Natl Acad Sci USA* **117**, 26406–26413 (2020).

690 45. Dabrowska, J. *et al.* Striatal-enriched protein tyrosine phosphatase-STEPs toward
691 understanding chronic stress-induced activation of corticotrophin releasing factor
692 neurons in the rat bed nucleus of the stria terminalis. *Biol. Psychiatry* **74**, 817–826
693 (2013).

694 46. Hu, P. *et al.* Chronic Stress Induces Maladaptive Behaviors by Activating Corticotropin-
695 Releasing Hormone Signaling in the Mouse Oval Bed Nucleus of the Stria Terminalis. *J.*
696 *Neurosci.* **40**, 2519–2537 (2020).

697 47. Daniel, S. E. *et al.* Chronic stress induces cell type-selective transcriptomic and
698 electrophysiological changes in the bed nucleus of the stria terminalis.
699 *Neuropharmacology* **150**, 80–90 (2019).

700 48. Wanat, M. J., Bonci, A. & Phillips, P. E. M. CRF acts in the midbrain to attenuate
701 accumbens dopamine release to rewards but not their predictors. *Nat. Neurosci.* **16**,
702 383–385 (2013).

703 49. Salimando, G. J., Hyun, M., Boyt, K. M. & Winder, D. G. BNST GluN2D-Containing NMDA
704 Receptors Influence Anxiety- and Depressive-like Behaviors and ModulateCell-Specific
705 Excitatory/Inhibitory Synaptic Balance. *J. Neurosci.* **40**, 3949–3968 (2020).

706 50. Hartley, N. D. *et al.* Dynamic remodeling of a basolateral-to-central amygdala
707 glutamatergic circuit across fear states. *Nat. Neurosci.* **22**, 2000–2012 (2019).

708 51. Sanford, C. A. *et al.* A Central Amygdala CRF Circuit Facilitates Learning about Weak
709 Threats. *Neuron* **93**, 164–178 (2017).

710 52. Rodríguez-Sierra, O. E., Turesson, H. K. & Pare, D. Contrasting distribution of
711 physiological cell types in different regions of the bed nucleus of the stria terminalis. *J.*
712 *Neurophysiol.* **110**, 2037–2049 (2013).

713 53. Gungor, N. Z. & Paré, D. Functional heterogeneity in the bed nucleus of the stria
714 terminalis. *J. Neurosci.* **36**, 8038–8049 (2016).

715 54. Zhan, J., Komal, R., Keenan, W. T., Hattar, S. & Fernandez, D. C. Non-invasive Strategies
716 for Chronic Manipulation of DREADD-controlled Neuronal Activity. *J. Vis. Exp.* (2019)
717 doi:10.3791/59439.

718 55. Schalbetter, S. M. *et al.* Oral application of clozapine-N-oxide using the micropipette-
719 guided drug administration (MDA) method in mouse DREADD systems. *Lab Anim (NY)*
720 **50**, 69–75 (2021).

721 56. Wess, J., Nakajima, K. & Jain, S. Novel designer receptors to probe GPCR signaling and
722 physiology. *Trends Pharmacol. Sci.* **34**, 385–392 (2013).

723 57. Walker, D. L., Miles, L. A. & Davis, M. Selective participation of the bed nucleus of the
724 stria terminalis and CRF in sustained anxiety-like versus phasic fear-like responses. *Prog*
725 *Neuropsychopharmacol Biol Psychiatry* **33**, 1291–1308 (2009).

726 58. Tran, L., Schulkin, J. & Greenwood-Van Meerveld, B. Importance of CRF receptor-
727 mediated mechanisms of the bed nucleus of the stria terminalis in the processing of
728 anxiety and pain. *Neuropsychopharmacology* **39**, 2633–2645 (2014).

729 59. Lee, Y., Fitz, S., Johnson, P. L. & Shekhar, A. Repeated stimulation of CRF receptors in the
730 BNST of rats selectively induces social but not panic-like anxiety.
731 *Neuropsychopharmacology* **33**, 2586–2594 (2008).

732 60. Dedic, N. *et al.* Deletion of CRH From GABAergic Forebrain Neurons Promotes Stress
733 Resilience and Dampens Stress-Induced Changes in Neuronal Activity. *Front. Neurosci.*
734 **13**, 986 (2019).

735 61. Wang, Y. *et al.* Single-cell morphological characterization of CRH neurons throughout the
736 whole mouse brain. *BMC Biol.* **19**, 47 (2021).

737 62. Chen, P. *et al.* Prefrontal Cortex Corticotropin-Releasing Factor Neurons Control
738 Behavioral Style Selection under Challenging Situations. *Neuron* **106**, 301-315.e7 (2020).

739 63. Elliott, E., Ezra-Nevo, G., Regev, L., Neufeld-Cohen, A. & Chen, A. Resilience to social
740 stress coincides with functional DNA methylation of the Crf gene in adult mice. *Nat.*
741 *Neurosci.* **13**, 1351–1353 (2010).

742 64. Lemos, J. C. *et al.* Severe stress switches CRF action in the nucleus accumbens from
743 appetitive to aversive. *Nature* **490**, 402–406 (2012).

744 65. Zhang, H. *et al.* α1- and β3-Adrenergic Receptor-Mediated Mesolimbic Homeostatic
745 Plasticity Confers Resilience to Social Stress in Susceptible Mice. *Biol. Psychiatry* **85**, 226–
746 236 (2019).

747 66. Friedman, A. K. *et al.* Enhancing depression mechanisms in midbrain dopamine neurons
748 achieves homeostatic resilience. *Science* **344**, 313–319 (2014).

749 67. Bagot, R. C. *et al.* Circuit-wide Transcriptional Profiling Reveals Brain Region-Specific
750 Gene Networks Regulating Depression Susceptibility. *Neuron* **90**, 969–983 (2016).

751 68. Dabrowska, J., Hazra, R., Guo, J.-D., Dewitt, S. & Rainnie, D. G. Central CRF neurons are
752 not created equal: phenotypic differences in CRF-containing neurons of the rat
753 paraventricular hypothalamus and the bed nucleus of the stria terminalis. *Front.*
754 *Neurosci.* **7**, 156 (2013).

755 69. Justice, N. J., Yuan, Z. F., Sawchenko, P. E. & Vale, W. Type 1 corticotropin-releasing
756 factor receptor expression reported in BAC transgenic mice: implications for reconciling
757 ligand-receptor mismatch in the central corticotropin-releasing factor system. *J. Comp.*
758 *Neurol.* **511**, 479–496 (2008).

759 70. Ramot, A. *et al.* Hypothalamic CRFR1 is essential for HPA axis regulation following
760 chronic stress. *Nat. Neurosci.* **20**, 385–388 (2017).

761 71. McClard, C. K. *et al.* POU6f1 Mediates Neuropeptide-Dependent Plasticity in the Adult
762 Brain. *J. Neurosci.* **38**, 1443–1461 (2018).

763 72. Hillhouse, E. W. & Grammatopoulos, D. K. The molecular mechanisms underlying the
764 regulation of the biological activity of corticotropin-releasing hormone receptors:
765 implications for physiology and pathophysiology. *Endocr. Rev.* **27**, 260–286 (2006).

766 73. Partridge, J. G. *et al.* Stress increases GABAergic neurotransmission in CRF neurons of
767 the central amygdala and bed nucleus stria terminalis. *Neuropharmacology* **107**, 239–
768 250 (2016).

769 74. Spierling, S. R. & Zorrilla, E. P. Don't stress about CRF: assessing the translational failures
770 of CRF1antagonists. *Psychopharmacology (Berl)* **234**, 1467–1481 (2017).

771 75. Waters, R. P. *et al.* Evidence for the role of corticotropin-releasing factor in major
772 depressive disorder. *Neurosci. Biobehav. Rev.* **58**, 63–78 (2015).

773 76. Reul, J. Corticotropin-releasing factor receptors 1 and 2 in anxiety and depression. *Curr.*
774 *Opin. Pharmacol.* **2**, 23–33 (2002).

775 77. Johnson, S. B. *et al.* A basal forebrain site coordinates the modulation of endocrine and
776 behavioral stress responses via divergent neural pathways. *J. Neurosci.* **36**, 8687–8699
777 (2016).

778 78. Crestani, C. C., Alves, F. H. F., Correa, F. M. A., Guimarães, F. S. & Joca, S. R. L. Acute
779 reversible inactivation of the bed nucleus of stria terminalis induces antidepressant-like
780 effect in the rat forced swimming test. *Behav. Brain Funct.* **6**, 30 (2010).

781 79. Fiedler, D. *et al.* Brain-Derived Neurotrophic Factor/Tropomyosin Receptor Kinase B
782 Signaling Controls Excitability and Long-Term Depression in Oval Nucleus of the BNST. *J.*
783 *Neurosci.* **41**, 435–445 (2021).

784 80. Cathomas, F., Murrough, J. W., Nestler, E. J., Han, M.-H. & Russo, S. J. Neurobiology of
785 resilience: interface between mind and body. *Biol. Psychiatry* **86**, 410–420 (2019).

786 81. Koo, J. W., Chaudhury, D., Han, M.-H. & Nestler, E. J. Role of Mesolimbic Brain-Derived
787 Neurotrophic Factor in Depression. *Biol. Psychiatry* **86**, 738–748 (2019).

788 82. Wook Koo, J. *et al.* Essential Role of Mesolimbic Brain-Derived Neurotrophic Factor in
789 Chronic Social Stress-Induced Depressive Behaviors. *Biol. Psychiatry* **80**, 469–478 (2016).

790 83. Takahashi, D. *et al.* Tonic Suppression of the Mesolimbic Dopaminergic System by
791 Enhanced Corticotropin-Releasing Factor Signaling Within the Bed Nucleus of the Stria
792 Terminalis in Chronic Pain Model Rats. *J. Neurosci.* **39**, 8376–8385 (2019).

793 84. Caillé, S., Guillem, K., Cador, M., Manzoni, O. & Georges, F. Voluntary nicotine
794 consumption triggers in vivo potentiation of cortical excitatory drives to midbrain
795 dopaminergic neurons. *J. Neurosci.* **29**, 10410–10415 (2009).

796 85. Silberman, Y., Matthews, R. T. & Winder, D. G. A corticotropin releasing factor pathway
797 for ethanol regulation of the ventral tegmental area in the bed nucleus of the stria
798 terminalis. *J. Neurosci.* **33**, 950–960 (2013).

799 86. Rodaros, D., Caruana, D. A., Amir, S. & Stewart, J. Corticotropin-releasing factor
800 projections from limbic forebrain and paraventricular nucleus of the hypothalamus to
801 the region of the ventral tegmental area. *Neuroscience* **150**, 8–13 (2007).

802 87. Dong, H. W., Petrovich, G. D., Watts, A. G. & Swanson, L. W. Basic organization of
803 projections from the oval and fusiform nuclei of the bed nuclei of the stria terminalis in
804 adult rat brain. *J. Comp. Neurol.* **436**, 430–455 (2001).

805 88. Maita, I., Bazer, A., Blackford, J. U. & Samuels, B. A. Functional anatomy of the bed
806 nucleus of the stria terminalis-hypothalamus neural circuitry: Implications for valence

807 surveillance, addiction, feeding, and social behaviors. *Handb. Clin. Neurol.* **179**, 403–418
808 (2021).

809 89. Kaouane, N., Ada, S., Hausleitner, M. & Haubensak, W. Dorsal Bed Nucleus of the Stria
810 Terminalis-Subcortical Output Circuits Encode Positive Bias in Pavlovian Fear and
811 Reward. *Front. Neural Circuits* **15**, 772512 (2021).

812 90. Cao, J.-L. *et al.* Mesolimbic dopamine neurons in the brain reward circuit mediate
813 susceptibility to social defeat and antidepressant action. *J. Neurosci.* **30**, 16453–16458
814 (2010).

815 91. Morel, C. *et al.* Midbrain projection to the basolateral amygdala encodes anxiety-like but
816 not depression-like behaviors. *Nat. Commun.* **13**, 1532 (2022).

817 92. Kumar, S. *et al.* Prefrontal cortex reactivity underlies trait vulnerability to chronic social
818 defeat stress. *Nat. Commun.* **5**, 4537 (2014).

819 93. Friedman, A. K. *et al.* KCNQ channel openers reverse depressive symptoms via an active
820 resilience mechanism. *Nat. Commun.* **7**, 11671 (2016).

821 94. Chaudhury, D. *et al.* Rapid regulation of depression-related behaviours by control of
822 midbrain dopamine neurons. *Nature* **493**, 532–536 (2013).

823 95. Xiao, Q. *et al.* A new GABAergic somatostatin projection from the BNST onto accumbal
824 parvalbumin neurons controls anxiety. *Mol. Psychiatry* **26**, 4719–4741 (2021).

825 96. Cooper, M. A. & Huhman, K. L. Blocking corticotropin-releasing factor-2 receptors, but
826 not corticotropin-releasing factor-1 receptors or glucocorticoid feedback, disrupts the
827 development of conditioned defeat. *Physiol. Behav.* **101**, 527–532 (2010).

828 97. Challis, C. *et al.* Raphe GABAergic neurons mediate the acquisition of avoidance after
829 social defeat. *J. Neurosci.* **33**, 13978–88, 13988a (2013).

830 98. Challis, C., Beck, S. G. & Berton, O. Optogenetic modulation of descending
831 prefrontocortical inputs to the dorsal raphe bidirectionally bias socioaffective choices
832 after social defeat. *Front. Behav. Neurosci.* **8**, 43 (2014).

833 99. Calipari, E. S. *et al.* Dopaminergic dynamics underlying sex-specific cocaine reward. *Nat.*
834 *Commun.* **8**, 13877 (2017).

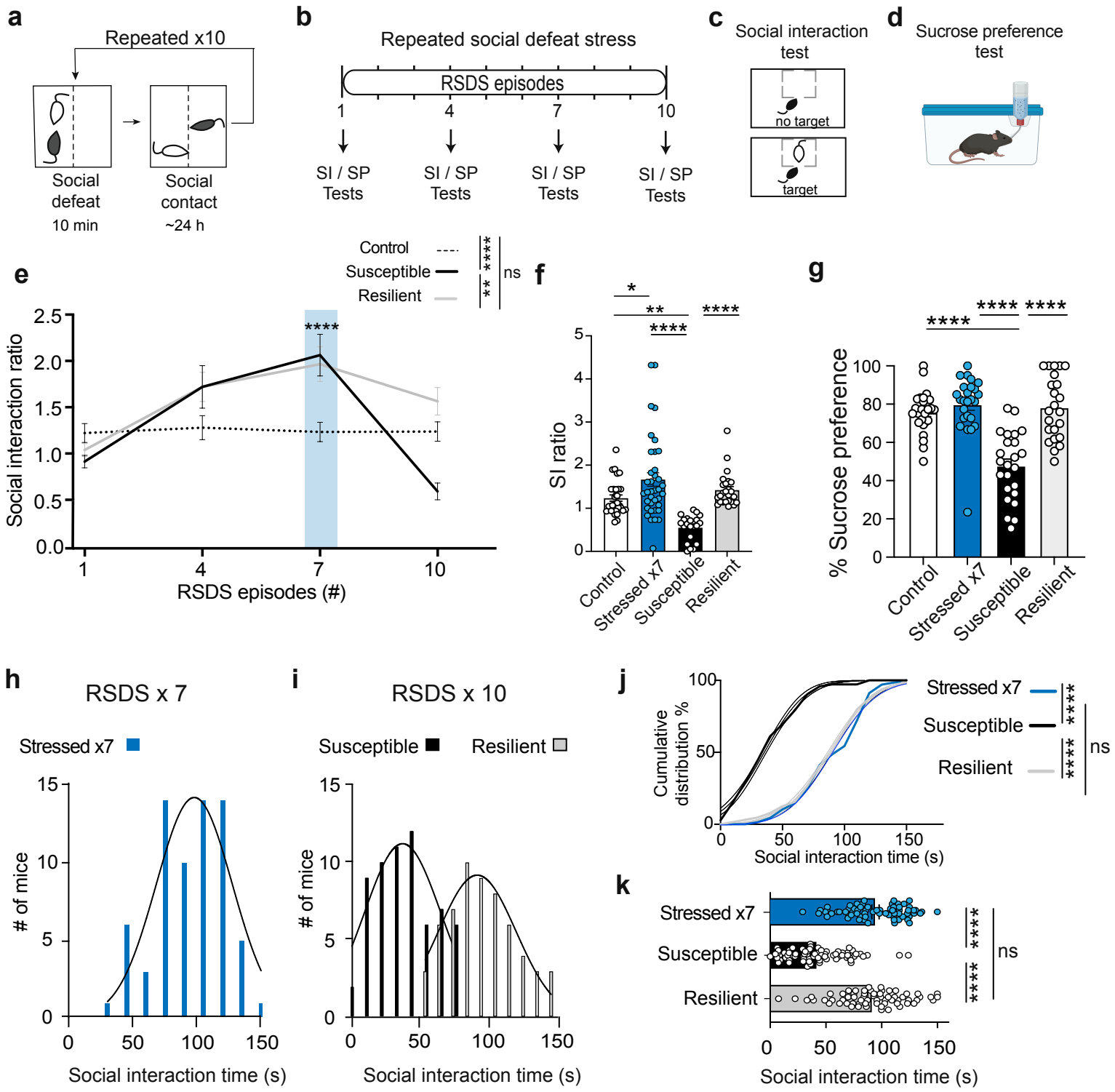

Susceptible and resilient subgroups emerge between 7 and 10 daily episodes of social defeat stress

Figure 1

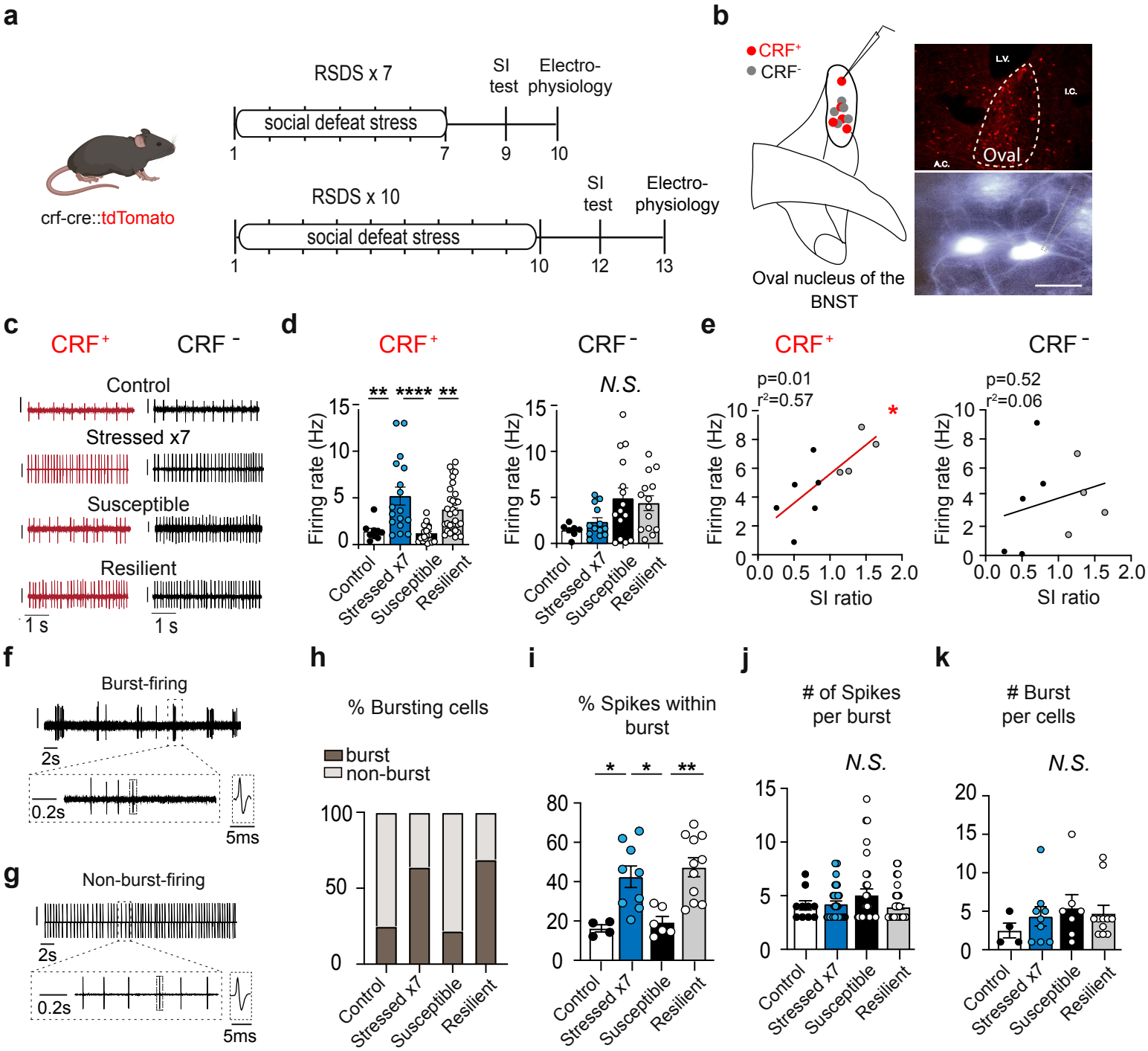

Firing rate alterations in BNSTov^{CRF} neurons occur as adaptation to social stress, persisting in resilient, not susceptible mice.

Figure 2

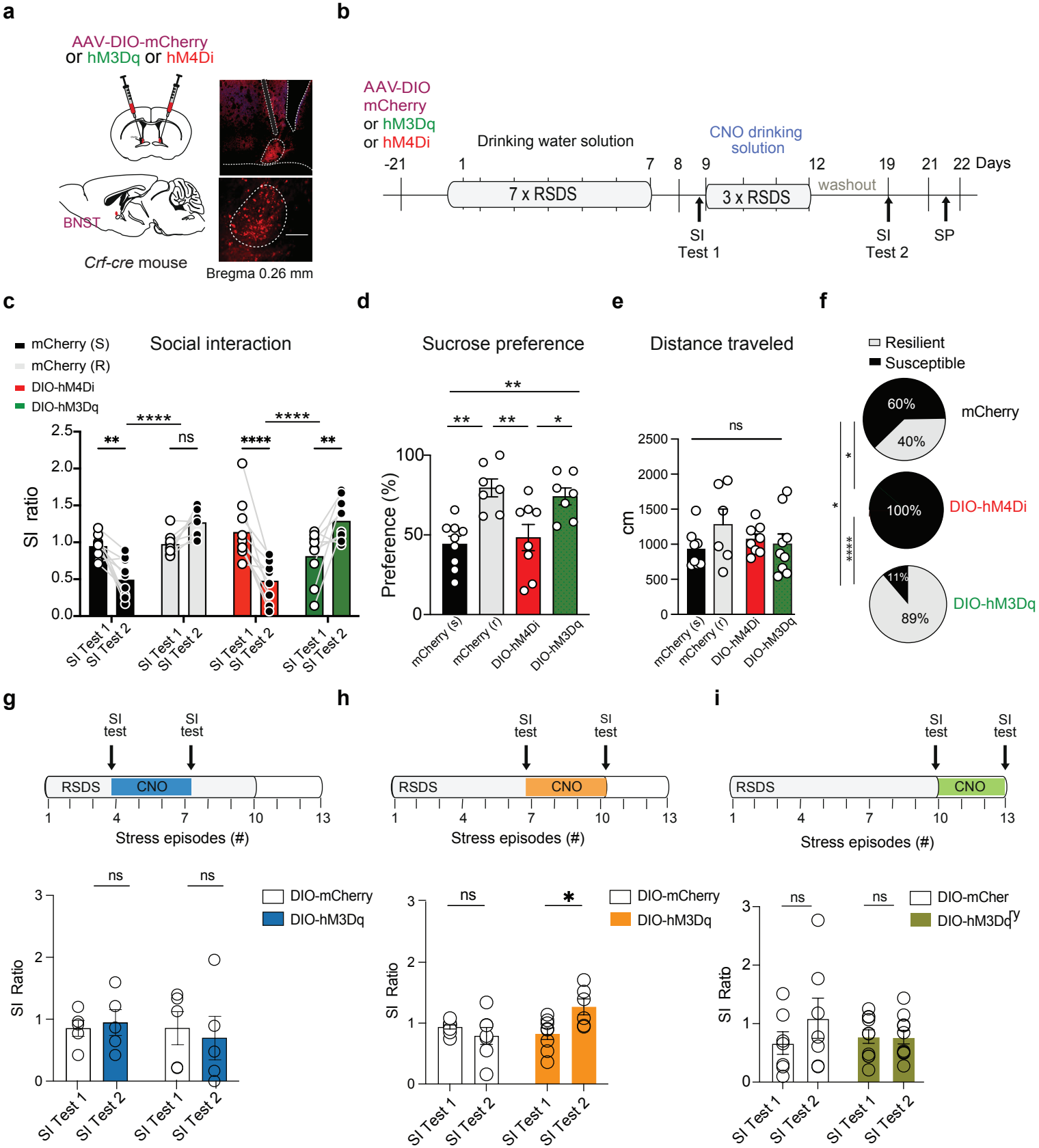

Chemogenetic Modulation of BNSTov^{CRF} Neurons Recapitulates Behavioural Tipping Point

Figure 3

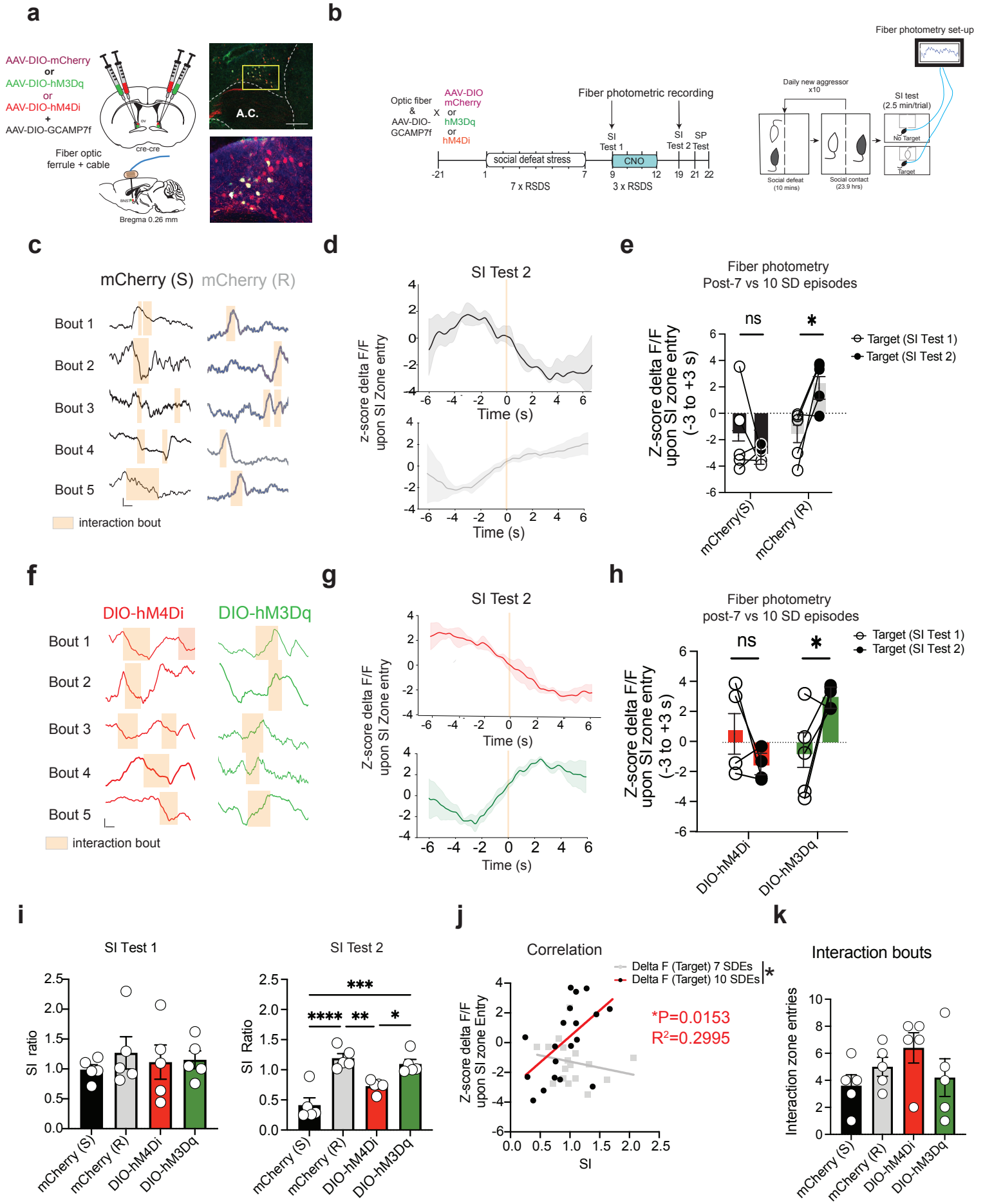

BNSTov^{CRF} calcium-dynamics encode stress effect on social interaction

Figure 4

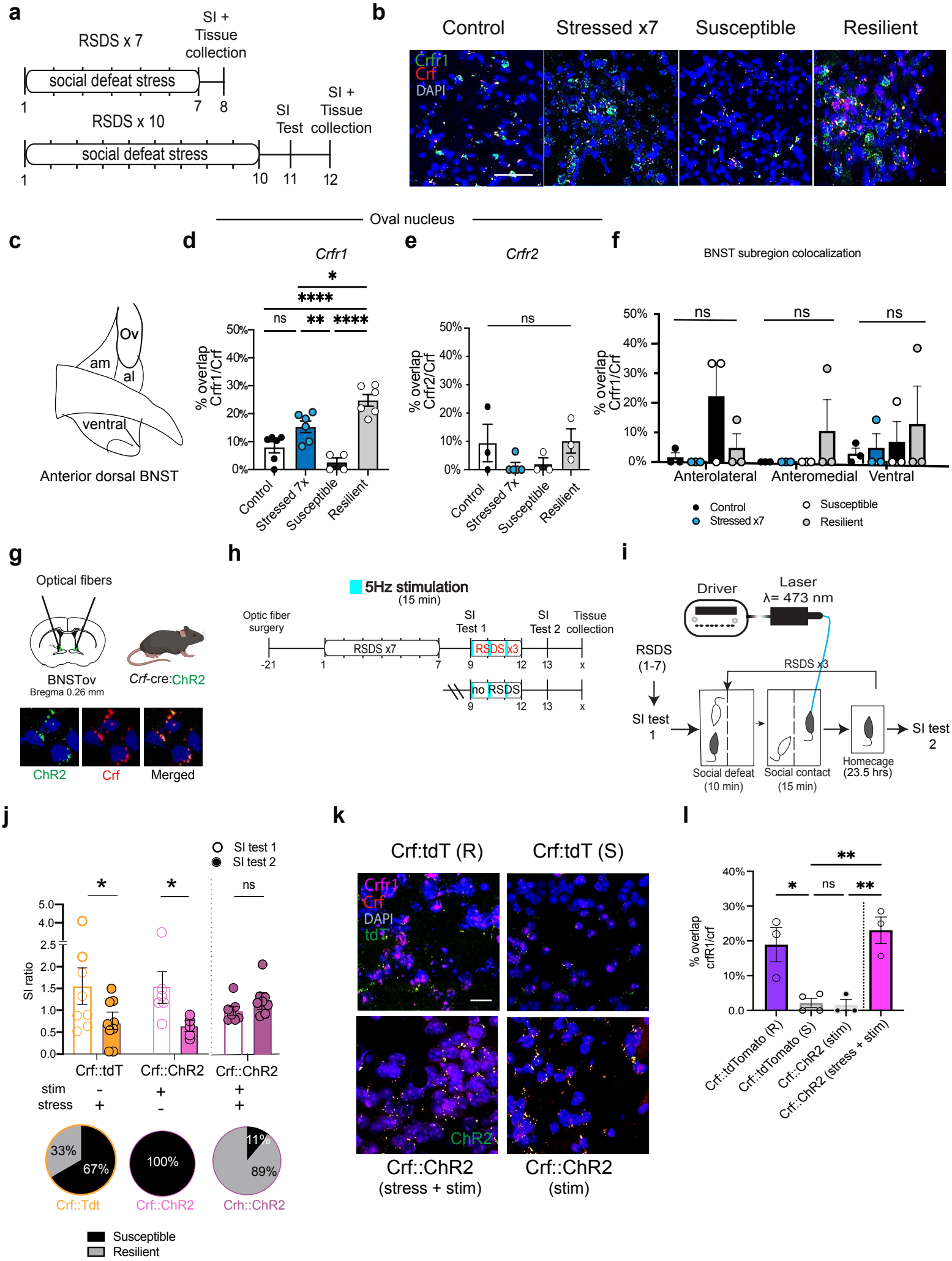

BNSTov *Crfr1* is associated with the emergence of resiliency

Figure 5

Figure 1. Susceptible and resilient subgroups emerge between 7 and 10 daily episodes of social defeat stress.

a, Experimental design for repeated social defeat stress (RSDS). **b,** Experimental timeline of social defeat stress and behavioral tests: social interaction (SI) and sucrose preference (SP). **c,** Social interaction test schema involving target and no target trials. **d,** Sucrose preference test schematic. **e,** Effect of cumulative social defeat stress on social interaction measured as SI ratios, after 1, 4, 7, and 10 social defeat episodes (SDEs) (n=11-18 mice/group), two-way ANOVA interaction $F_{(6,134)}$=5.783, ****P<0.0001, row factor $F_{(3,134)}$=12.11, ****P<0.0001, $F_{(2,134)}$=4.086, column factor *P<0.05, Tukey's post-hoc test susceptible vs resilient ****P<0.0001, susceptible vs control **P<0.01, resilient vs control P=0.2751. SI test susceptible (SI test stressed x7 vs stressed x10) ****P<0.0001. **f,** Aggregated data on social interaction test across experiments. One-way ANOVA treatment $F_{(3,109)}$=14.61, ****P<0.0001. Tukey's post-hoc test control vs stressed x7 *P<0.05, control vs susceptible **P<0.01, stressed x7 vs susceptible ****P<0.0001, susceptible vs resilient ****P<0.0001 (n=25-37 mice). **g,** Sucrose preference test. One-way ANOVA treatment $F_{(3,93)}$=24.06, ****P<0.0001). Tukey's post-hoc test control vs stressed x7 P=0.77, control vs susceptible ****P<0.0001, control vs resilient P=0.9387, stressed x7 vs susceptible ****P<0.0001, stressed x7 vs resilient P=0.984, susceptible vs resilient ****P<0.0001 (n=23-25 mice). **h,** Distribution of stressed mice who underwent 7 SDEs. **i,** Distribution of mice who underwent 10 SDEs and sorted into susceptible and resilient mice**. j,** Cumulative distribution of all stressed mice. Kolmogorov-Smirnov (distance) 0.2054 Susceptible vs Resilient, ****P<0.0001. **k,** Time spent interaction socially with a novel conspecific. One-Way ANOVA $F_{(2,201)}$=76.63, ****P<0.0001. Tukey's

post-hoc susceptible vs resilient ***P<0.001, susceptible vs stressed x7 ****P<0.0001, stressed vs resilient P=0.4984 (n=72 susceptible, 64 resilient mice). All data represent means ± SEM. *P < 0.05, **P < 0.01, ***P < 0.001, ****P<0.0001, ns = not significant.

Figure 2. Firing rate alterations in BNSTov^{CRF} neurons occur as adaptation to social stress, persisting in resilient, not susceptible mice.

a, Mouse genotype and timeline of cell-attached electrophysiology experiments**. b,** Fluorescence-guided cell-attached electrophysiology setup, brain slice of the BNST (CRF cells, tdTomato) and DIC image of CRF neurons, scale bar 0.63 mm. **c,** Representative trace of BNSTov^{CRF} positive and negative neurons of control, stressed (SDEs x 7), susceptible, and resilience mice. **d,** Firing rate of CRF^{+} neurons (n=9-31 cells/group), ****P<0.0001, one-way ANOVA, Tukey's multiple comparison's test, control vs stressed (SDEs x 7) **P<0.01, susceptible vs resilient **P<0.01, susceptible vs stressed (SDEs x7), ****P<0.0001. Firing rate of CRF^{-} neurons (n=7-15 cells per 4-6 mice/group), one-way NOVA, $F_{(3,\ 45)}$=3.113, *P<0.05, Tukey's multiple comparison's test, control vs stressed x7 P=0.9192, control vs susceptible P=0.0769, control vs resilient P=0.1742, stressed (SDEs x 7) vs susceptible P=0.1370, stressed x7 vs resilient P=0.3219, susceptible vs resilient P=0.9673. **e,** Correlation of firing rate with social interaction ratio: CRF^{+}, R^2=0.5726, *P<0.05; CRF^{-}, R^2=0.0609, P=0.5219. **f,** Representative sample of burst firing. **g,** Representative sample of tonic firing. **h,** Percentage of bursting cells per animal group. **i**, Percentage of spikes within burst. **j,** Number of spikes per burst. **k,**

Number of bursts per cell. (n=10-52 cells per 4-6 mice/group). All data represent means ± SEM. *P<0.05, **P<0.01, ***P<0.001, ****P<0.0001, ns = not significant.

Figure 3. Chemogenetic modulation of BNSTov^{CRF} neurons bidirectional recapitulates behavioural tipping point.

a, Viral targeting of BNSTov. **b,** Experimental design of chemogenetic manipulation of BNSTov neurons with CNO-drinking water construct. **c,** Social interaction test, two-way ANOVA $F_{(3,68)}$=18.01, row ****P<0.0001, row factor $F_{(3, 68)}$=9.965, P=0.2616 (time), row factor x time $F_{(1,68)}$=1.281, ****P<0.0001, Sidak's multiple comparisons test mCherry (s), **P=0.0017 (n=10 mice); mCherry (r), P=0.1322 (n=9 mice); hM4Di, ****P<0.0001 (n=10 mice); hM3Dq, **P=0.0018 (n=9 mice). **d,** Sucrose preference test. one-way ANOVA treatment $F_{(3,27)}$=8.310, ***P<0.001, Tukey's post-hoc testing susceptible vs hM4Di, P=9619; susceptible vs resilient, **P<0.01; susceptible vs hM3Dq, **P<0.01; hM4Di vs resilient, **P<0.01; hM4Di vs hM3Dq, *P<0.05; resilient vs hM3Dq P=0.9368 (7-9 mice per group). **e,** Distance traveled, one-way ANOVA $F_{(3,27)}$=1.031, P=0.3944. **f,** Percentage of susceptible or resilient mice: DIO-hM4Di, 100% susceptible; DIO-hM3Dq, 89% resilient and 11% susceptible; mCherry, 40% resilient and 60% susceptible. Chi-square test=15.66, df=2, ***P<0.001 (n=21 mCherry, 10 hMDi, 9 hM3Dq); Fisher's post-hoc test mCherry vs hM4Di, *P<0.05; mCherry vs hM3Dq, *P<0.05; hM4Di vs hM3Dq, ****P<0.0001. **g,** Repeated social defeat DREADDs manipulation (4-7 episodes of stress), 2-way ANOVA treatment $F_{(1,16)}$=0.01749, P=0.8964; SI Test 1 vs SI Test 2,

$F_{(1,16)}$=0.2377, P=0.6325; interaction $F_{(1,16)}$=0.07055, P=0.6218 (n=5-6 mice/group). **h,** RSDS DREADDs manipulation (7-10 episodes of stress), 2-way ANOVA treatment, $F_{(1,22)}$=8.675, **P< 0.01; SI Test 1 vs SI Test 2, $F_{(1,22)}$=2.549, P=0.1247; interaction $F_{(1,22)}$=2.549, P=0.1247. Sidak's post-hoc test SI Test 1 vs SI Test 2, control, P=0.5533; DIO-hM3Dq, *P<0.05 (n=6-7 mice/group). **i,** RSDS DREADDs manipulation (10-13 episodes of stress), 2-way ANOVA $F_{(1,30)}$=1.192, treatment, P=0.2623. SI Test 1 vs Si Test 2, $F_{(1,30)}$=0.3132, P=0.2836. Interaction $F_{(1,30)}$=0.2623, P=0.5799. All data represent means ± SEM. *P<0.05, **P<0.01, ***P<0.001, ****P<0.0001, ns = not significant.

Figure 4. BNSTov^{CRF} calcium-dynamics encode stress effect on social interaction

a, Viral targeting of the BNSTov. **b**, Experimental design of multiplexed chemogenetics with drinking water-CNO delivery and fiber photometry. **c,f,** Representative calcium recordings of mCherry susceptible (S), mCherry resilient (R), hM3Dq, and hM4Di groups, respectively. Vertical scale bar is equal to z-score of 1, and horizontal scale bar is equal to 10 s. **d**, **g**, Representative averaged trace centered around interaction bout for the four groups stated above. **e,** Two-way RM ANOVA row factor $F_{(3,14)}$=1.401; pre vs post-CNO $F_{(1,14)}$=0.8179; subject $F_{(14,14)}$=1.195; Row x SI Test 1/SI Test 2, $F_{(3, 14)}$=9.343, **P<0.01. Sidak's post-hoc test, susceptible vs resilient, P=0.137 vs *P=0.05, respectively (n=4 mice/group). **h,** hM4Di vs hM3Dq, P=0.3069 vs *P<0.05, respectively (n=4-5 mice/grp). **i**, SI Test 1 social interaction test. One-way ANOVA $F_{(3,16)}$=0.291, P=0.8308 (n=5 mice/group). SI Test 2 social interaction test, One-Way ANOVA $F_{(3,16)}$=17.83, ****P<0.0001; Tukey's post-hoc test, susceptible vs resilient, ****P<0.0001; susceptible

vs hM3Dq, ***P<0.001; susceptible vs hM4Di, P=0.0762; resilient vs hM3Dq, P=0.8506; resilient vs HM4Di, **P<0.01; hM3Dq vs hM4Di, *P<0.05 (n=5 mice/group). **j**, Correlation of SI ratio and z-score delta F/F upon social entry, simple linear regression pre-CNO $F_{(1,15)}$=0.7674, P=0.3948; SI test 2 $F_{(1,17)}$=7.268, *P<0.05. Intersection of lines, $F_{(1,32)}$=6.896, *P<0.05 (n=18 mice). **k**, Number of social interaction bouts, one-way ANOVA $F_{(3,16)}$=1.346, P=0.2949 (n=5 mice/group). All data represent means ± SEM. *P<0.05, **P<0.01, ***P<0.001, ****P<0.0001, ns = not significant.

Figure 5. BNSTov *Crfr1* is associated with the emergence of resiliency

a, Experimental timeline of RNAScope *in situ* hybridization of mice that underwent social defeat stress. **b**, Representative images of control, stressed x7, susceptible, and resilient. 20x magnification, scale bar 0.64 mm. **c**, Schematic of anterior dorsal BNST. **d**, *Crfr1* mRNA colocalization, one-way ANOVA $F_{(3,18)}$=20.91, ****P<0.0001; Tukey's posthoc test, control vs stressed x7, P=0.0701; control vs susceptible, P=0.3336; control vs resilient, ****P<0.0001; stressed x7 vs susceptible, **P<0.01; stressed x7 vs resilient, *P<0.05; susceptible vs resilient, ****P<0.0001 (n=4-6 BNST brain samples). **e**, *Crfr2* mRNA colocalization, one-way ANOVA $F_{(3,10)}$=1.790, P=0.2166 (n=3 BNST brain samples). **f,** RNAscope BNST subregion comparison, two-way ANOVA interaction $F_{(6,24)}$=1.057, P=0.4147; row factor $F_{(2,24)}$=0.6092, P=0.5520; column factor $F_{(3,24)}$=1.549, P=0.2275 (n=3 BNST brain samples). **g**, Viral injection site. **h**, Experimental timeline. **i**, Optogenetic and social behavioral setup. **j**, Optogenetics social interaction, two-way ANOVA interaction $F_{(1,28)}$=5.059, *P<0.05; row factor $F_{(1,28)}$=1.061e-005, P=0.9974; column factor

$F_{(1,28)}$=1.419, P=0.2436. Sidak's post-hoc test, *Crf*::tdT, *P<0.05; *Crf*::ChR2, P=0.7233 (n=7-9 mice/group). Optogenetic manipulation unpaired t-test, *Crf*::tdT, t=2.556, df=40, *P<0.05 (n=8-9 mice); *Crf*::ChR2, t=0.7758, df=40, P=0.442457 (n=8-9 mice); *Crf*::ChR2, t=2.369, df=40, *P<0.05 (n=6 mice). Holm-Sidak method for multiple comparisons. **k**, Representative image, scale bar 0.64mm. **l**, Optogenetics-RNAScope experiment. One-Way ANOVA $F_{(3,9)}$=13.53, **P<0.01. Tukey's post-hoc test, *Crf*::ChR2 (stress + stim) vs *Crf*::tdT (resilient), P=0.7872; *Crf*::ChR2 (stress + stim) vs. *Crf*::tdTomato (s), **P<0.01; *Crf*::ChR2 (stress + stim) vs. *Crf*::chR2 (stim), **P<0.01; *Crf:*:tdTomato (r) vs. *Crf:*:tdTomato (s), *P<0.05; *Crf*::tdTomato (r) vs. *Crf:*:ChR2 (stim), *P<0.05; *Crf*::tdTomato (s) vs. *Crf*::ChR2 (stim), P=0.9988. All data represent means ± SEM. *P<0.05, **P<0.01, ***P<0.001, ****P<0.0001, ns = not significant.